PHYSICAL REVIEW B VOLUME 19, NUMBER 10 15 MAY 1979

Photoemission spectra and band structures of d-band metals. VII. Extensions of the combined interpolation scheme

N. V. Smith
Bell Laboratories, Murray Hill, New Jersey 07974

(Received 5 January 1979)

The combined interpolation scheme for face-centered-cubic d-band metals has been extended to higher energies ($\sim$1.6 Ry above the Fermi level) by inclusion of more plane waves in the basis set. Momentum matrix elements are evaluated for Cu from k-space derivatives of the Hamiltonian, and are used to calculate the imaginary part of the dielectric constant ϵ_2. Good agreement with the first-principles results of Janak, Williams, and Moruzzi is obtained. Momentum matrix elements corresponding to normal emission from Cu(111) and Cu(100) are calculated and are shown to be consistent with elementary atomic-dipole selection-rule considerations. The occurrence of hybridization nodes in the momentum matrix elements is reported and discussed.

I. INTRODUCTION

Earlier papers in this series[1,2] have been concerned with the interpretation of angle-integrated photoemission spectra from d-band metals using a combined interpolation scheme. This work was limited to the photon energy range $\hbar\omega \lesssim 12$ eV. In the intervening years there have been some very substantial advances in experimental technique. Specific advances are the development of angle-resolved photoemission, the extension to higher photon energies, and the use of the polarized synchrotron-radiation continuum.[3] The extent to which this abundance of new and incisive data can also be accounted for in terms of the combined-interpolation-scheme approach is of considerable interest. Such work would provide refined determinations of the bulk band structures and, by a process of elimination, would reveal those features of the spectra due to surface rather than bulk photoemission processes. To perform the work it was found necessary to extend the capabilities of the combined interpolation scheme described in an earlier paper by Smith and Mattheiss[1] (hereafter referred to as I). These extensions are the subject matter of this paper. Comparisons with experimental photoemission spectra will be made in subsequent papers.

Two main modifications of the scheme were required. The first was the extension of the scheme to higher electron energies. This was done by the inclusion of more plane waves in the basis set, and the details are described in Sec. II. The second modification is related to the intensities of peaks in the photoemission spectra. Formerly, an analysis of peaks positions was sufficient for a fairly complete interpretation. With the advent of angle-resolved photoemission, particularly with polarized light, the question of selection rules and intensities has come to the fore. Among the most important quantities determining intensities are the momentum matrix elements between occupied and unoccupied states. To calculate these we have used a formula which relates the momentum operator to k-space derivatives of the Hamiltonian. This formula and some preliminary numerical results will be described and discussed in Sec. III. The numerical work was performed on Cu, since first-principles calculations of both the bands and momentum matrix elements had been performed earlier for this metal by Janak, Williams, and Moruzzi[4] (JWM). These first-principles calculations provide a most convenient standard against which to measure the performance of the second-principles method described in this paper. Numerical results will be presented in Sec. III for the imaginary part ϵ_2 of the dielectric function and for the momentum matrix elements appropriate to normal photoemission from the (100) and (111) faces of Cu.

II. PARAMETRIZED HAMILTONIAN

A. Basis states

The Hamiltonian for nonrelativistic combined interpolation schemes for d-band metals is expressed in the following standard form[1,5]:

$$H = \begin{pmatrix} H_{cc} & H_{cd} \\ H_{dc} & H_{dd} \end{pmatrix} . \tag{1}$$

H_{cc}, H_{cd}, and H_{dd} represent the plane-wave, the hybridization, and the tight-binding d blocks, respectively. Here and elsewhere in this paper, we shall adopt the nomenclature of I. All of these blocks retain the same parametrized form as in

I. However, H_{cc}, the plane-wave (or pseudopotential) block, has been extended to a 16×16 rather than 4×4 matrix.

In terms of the reduced wave vector $\vec{k}$, the 16 plane waves included in the basis set are those with wave vectors $\vec{k}_i=\vec{k}+\vec{G}_i$, where $\vec{G}_i$ runs over all eight reciprocal-lattice vectors of type $(2\pi/a)(1,1,1)$, all six of the type $(2\pi/a)(2,0,0)$, and the single vector $(2\pi/a)(-2,-2,0)$. This last vector is included for reasons of fuller symmetry as explained below. In the earlier scheme of I, based on only four plane waves, full symmetry was obtained only for the relatively low-lying plane-wave-like levels such as $\Gamma_1(0)$, L_2, L_1 $(0.75E_a)$, X_4, X_1 $(1.00E_a)$, and $W_1W_2W_3$ $(1.25E_a)$. [The numbers in parentheses are the free-electron energies of these levels expressed as multiples of E_a, where $E_a=(\hbar^2/2m)(2\pi/a)^2$ and a is the lattice constant. We are using also the representations appropriate to the nonrelativistic case.] In the present scheme based on 16 plane waves, the following additional complete sets of levels are reproduced: $\Gamma_1\Gamma_{15}\Gamma_{25'}\Gamma_{2'}$ $(3.00E_a)$; $\Gamma_1\Gamma_{12}\Gamma_{15}$ $(4.00E_a)$; $L_1L_{2'}L_3L_{3'}$ $(2.75E_a)$; $X_1X_3X_{5'}$ $(2.00E_a)$; $W_1W_{2'}W_3$ $(3.25E_a)$. Note that the sixteenth plane wave is required for completeness of the last set at W, and this was the reason for its inclusion. In principle, therefore, we are able to reproduce the band structure up to energies of about $4E_a$.

The elements of the plane-wave block of the Hamiltonian are expressed in the same form as in I:

$$H_{ij}=\alpha k_i^2\delta_{ij}+V_{ij}+Sj_2(k_iR)j_2(k_jR)P_2(\hat{k}_i\cdot\hat{k}_j)\ . \tag{2}$$

The last term is a nonlocal contribution to the pseudopotential which takes account of the strong effects due to orthogonalization of the plane-wave basis states to the tight-binding d states. The principal Fourier components V_{ij} of the local pseudopotential which enter into the 16 plane-wave scheme are V_{000}, V_{111}, V_{200}, V_{220}, V_{311}, V_{222}, and V_{400} and V_{420}. For convenience V_{400} and V_{420} are set equal to zero. The components V_{000}, V_{111}, and V_{200} were already present in the four-plane-wave scheme. The new scheme therefore introduces the new parameters V_{220}, V_{311}, and V_{222}, thus raising the total number of disposable parameters from 16 to 19.

As in I, the elements of the hybridization block are expressed in the form

$$H_{in}=B_{t,e}\,j_2(k_iR)Y_n(\hat{k}_i)\ . \tag{3}$$

The spherical Bessel functions $j_2(k_jR)$ which appear in both Eqs. (2) and (3) are actually approximations to certain integrals over the radial parts of the d wave functions.[5] We mention this here merely to alert the reader to the fact that this approximation may require improvements as the scheme is extended to higher energies, i.e., higher values of k_i and k_j.

B. Fits to first-principles band structures

To test the performance of the extended scheme, its parameters have been fitted by a nonlinear-least-squares method to the nonrelativistic band structure of Cu as calculated by JWM. The JWM calculation was performed by the Korringa-Kohn-Rostoker (KKR) method, and the bands were then stretched by 8% along the energy scale in order to obtain better agreement with angle-integrated photoemission spectra. Our fit was performed to the stretched rather than unstretched bands. The results of the fit are displayed in Table I. The parameters are defined in paper I, and are expressed in the same units.

For purposes of comparison, we also show in Table I the parameters obtained by fitting the earlier four-plane-wave scheme to the same band structure. The main difference is that the Fletcher-Wohlfarth parameters A_{1-6} are considerably smaller in the 16-plane-wave scheme. This is a

TABLE I. Parameters of the combined interpolation scheme obtained by fitting the stretched Cu band structure of Ref. 4: (a) 16-plane-wave scheme; (b) 4-plane-wave scheme.

	(a)	(b)
d Bands		
E	0.3714	0.3430
Δ	−0.0082	0.0033
A_1	0.01303	0.02086
A_2	0.00229	0.00596
A_3	0.00561	0.00803
A_4	0.00797	0.01213
A_5	0.00257	0.00313
A_6	0.00634	0.00949
Plane-wave		
α	0.01420	0.01501
V_{000}	−0.0785	−0.1437
V_{111}	0.0974	0.0713
V_{200}	0.1210	0.0928
V_{220}	0.0974	...
V_{311}	0.2004	...
V_{222}	0.1125	...
Orthogonality and hybridization		
R	0.334	(0.410)[a]
S	0.744	0.757
B_t	1.359	1.116
B_e	1.291	1.131

[a] Not treated as disposable.

consequence of the fact that in the 16-plane-wave scheme there is more opportunity for hybridization between the plane-wave and d states. The overall effect of the hybridization is to push the lower-energy d bands to lower energies relative to the upper d bands, thereby increasing the d-band width. These leave a smaller proportion of the d-band width to be accounted for by the d-d overlap embodied in the Fletcher-Wohlfarth parameters. The 19 parameters of the 16-plane-wave scheme were fitted to 39 energy levels. Th overall rms error was 0.015 Ry. For the lowest six bands the rms error was 0.008 Ry.

III. MOMENTUM MATRIX ELEMENTS

A. Basic expression

In the standard formalism of band theory, where the wave functions are expressed as Bloch functions, the momentum operator may be written in terms of the Hamiltonian operator[6]:

$$\vec{P} = \frac{m}{\hbar}\frac{\partial H(\vec{k})}{\partial \vec{k}} . \qquad (4)$$

In the combined interpolation scheme, the matrix elements of H are all given as analytic functions of $\vec{k}$. The momentum matrix is therefore obtainable by simple differentiation. Note that all the parameters which enter into H have been completely determined by fitting to the energy bands. We therefore have the important point that *the generation of* $\vec{P}$ *by the differentiation of* H *does not require the introduction of any additional disposable parameters*. In spite of the obvious appeal of such an approach, it does not seem to be widely recognized, and has been used on only a few occasions in the past.[7]

Expressed in terms closer to actual computational usage, momentum matrix elements between specific states are obtained as follows. Let u_{mf} (m=1–21) and u_{ni} (n=1–21) represent the eigenvectors associated, respectively, with the energy eigenvalues E_f and E_i generated at some point $\vec{k}$. (The 16 plane waves and 5 tight-binding d functions give a total of 21 basis states.) The three components of the momentum matrix element between these states are then given by

$$(P_{fi})_{x,y,z} = \frac{m}{\hbar}\sum_{m,n} u_{mf}\frac{\partial H_{mn}}{\partial k_{x,y,z}} u_{ni} . \qquad (5)$$

In other words, we apply to $\partial H/\partial\vec{k}$ the same unitary transformation which diagonalizes H.

B. Results for $\epsilon_2(\omega)$

In addition to the Cu energy bands, JWM also report numerical results for ϵ_2, the imaginary part of the dielectric constant. These first-principles calculations of ϵ_2 provide an excellent standard against which to test the performance of second-principles methods. JWM also present results for the band-by-band decomposition of ϵ_2 providing a more detailed test. Calculations of ϵ_2 and its band-by-band decomposition have been performed using the scheme of the present paper, and the comparisons with the first-principles results will now be made.

The standard expression for ϵ_2 is[8]

$$\epsilon_2(\omega) = \frac{e^2}{3\pi m^2\omega^2}\sum_{f,i}\int_{BZ} d^3k\,|P_{fi}|^2 \times \delta(E_f(\vec{k}) - E_i(\vec{k}) - \hbar\omega) . \qquad (6)$$

Note that Eq. (6) contains no further disposable parameters. This permits us to assess the performance of the present scheme in absolute as well as relative terms. The k-space integral in Eq. (6) was performed by a Monte Carlo method whose essential details are described in an earlier paper of the series.[2]

The numerical results for ϵ_2 are shown in Fig. 1(a) where they are compared with the experimental measurements of Beaglehole and Erlbach.[9] The overall agreement is good. The calculations reproduce the two principal maxima at about 2.5 and 5.0 eV, although the former is somewhat weaker and the latter somewhat stronger than those observed experimentally. Comparisons with a more extensive set of experimental data are to be found in the paper by JWM.

The band-by-band decompositions of the calculated ϵ_2 are shown in Fig. 1(b). These compare very favorably in general shape and magnitude with the first-principles results of JWM shown in Fig. 2. The contribution between bands 6 → 7 involves plane-wave-like initial states and plane-wave-like final states, at least in the energy range $\hbar\omega < 7$ eV. All the other contributions involve transitions between d-like initial states and plane-wave-like final states. In a constant matrix element approach, where $\omega^2\epsilon_2$ is related directly to the joint density of states, the various contributions 1 → 6 through 5 → 6 would be roughly equal in overall magnitude. It is seen, however, that the inclusion of momentum matrix elements enhances the 5 → 6 contribution and suppresses the 2 → 6 contribution relative to the other d → plane-wave contributions. The joint density of states of the 6 → 7 contribution is very small relative to the other contributions, since both initial- and final-state bands have steep slopes. With the inclusion of momentum matrix elements, however, the 6 → 7 contribution is comparable with, and even exceeds, the 1 → 6 contribution.

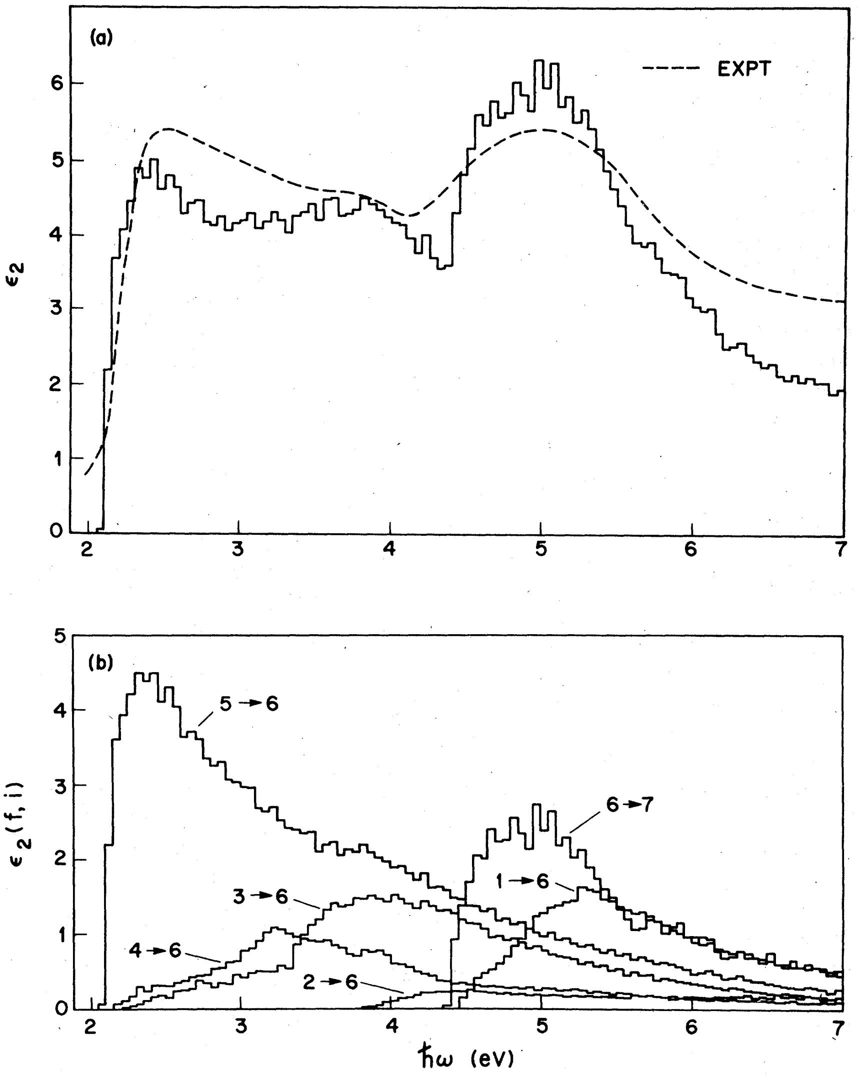

FIG. 1. Calculated values of ϵ_2: (a) comparison with experimental data of Ref. 9 (dashed curve); (b) band-to-band decomposition.

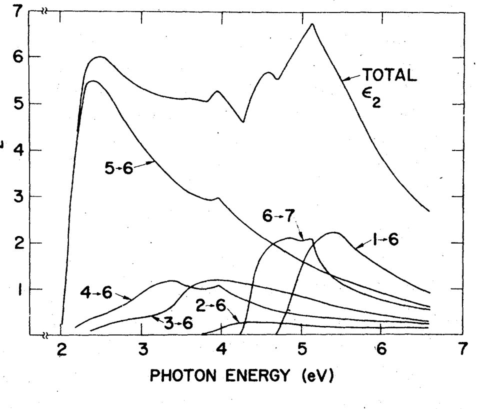

FIG. 2. First-principles calculations of ϵ_2 and its band-to-band decomposition by Janak, Williams, and Moruzzi (Ref. 4).

TABLE II. Comparison between the optical matrix elements $|P_{fi}|^2$ calculated by the first-principles method of JWM and the second-principle combined-interpolation-scheme method of this paper.

Transition	$\hbar\omega$ (Ry)	$\lvert P_{fi}\rvert^2/2m$ (Ry) JWM (Ref. 4)	$\lvert P_{fi}\rvert^2/2m$ (Ry) This work
$L_1 \rightarrow L_{2'}$	0.344	0.051	0.055
$L_3 \rightarrow L_{2'}$	0.214	0.012	0.006
$L_3 \rightarrow L_{2'}$	0.106	0.193	0.070
$L_{2'} \rightarrow L_1$	0.336	0.721	0.823
$X_1 \rightarrow X_{4'}$	0.540	0.042	0.051
$X_5 \rightarrow X_{4'}$	0.289	0.120	0.083
$X_{4'} \rightarrow X_1$	0.387	0.780	1.039

JWM also quote values of $|P_{if}|^2/2m$ for several critical-point transitions. These are listed in Table II, where they are compared with the values obtained by our second-principles method. In the case of degenerate levels, it is only the sum of the squares of the momentum matrix elements which is significant, and this is what is listed in Table II. The overall agreement is fair, especially when one considers that the values are distributed over two orders of magnitude. The strength of transitions from plane-wave-like levels ($L_{2'} \to L_1$, $X_{4'} \to X_1$) appears to be slightly overestimated by the present scheme. Transition strengths from d-like levels, on the other hand, tend to be underestimated, in some cases quite severely.

C. Normal photoemission from Cu(111) and Cu(100)

For photoelectrons propagating normal to a crystal surface we have $k_\parallel = 0$, where $k_\parallel$ is the component of the electron wave vector parallel to the surface. If we assume that $k_\parallel$ is conserved in crossing the surface, we are restricted to sampling those states along a line in k space perpendicular to the surface. For face-centered-cubic materials the [111] and [100] directions are particularly simple. We now analyze the behavior of $|P_{fi}|^2$ along these directions.

In normal emission from the (111) face we sample the ΓL line. The band structure along ΓL calculated by the combined interpolation scheme approach using the parameters of column (a) in Table I is shown in Fig. 3. Up to energies of about 2.2 Ry, the only unoccupied band capable of giving rise to external photoelectrons is the one of Λ_1 symmetry. The wave functions of states in this band are composed primarily of the two plane waves $\vec{k}$ and $\vec{k} + \vec{G}_{\bar{1}\bar{1}\bar{1}}$. Both these waves are propagating normal to the (111) surface, so the escape considerations are particularly favorable for photoelectrons excited into this band. Matrix elements for transitions into this Λ_1 band from the various occupied bands are shown in Fig. 3. The variations with the perpendicular component of the wave vector $k_\perp$ are also displayed, and it is seen that they are quite strong.

The matrix elements along ΓL have the following qualitative features. For transitions from the occupied Λ_1 levels $\vec{P}_{fi}$ is parallel to [111]; for transitions from the Λ_3 levels $\vec{P}_{fi}$ is perpendicular to [111]; these results required by parity selection rules. For transitions from the Λ_3 levels and the lower Λ_1 level, P_{fi} is zero at L. This is not surprising since these levels are predominantly d-like, whereas the final state, having L_1 symmetry, is s-like; the transitions are therefore forbidden according to atomic dipole selection rules. For the lower Λ_1 and the lower Λ_3 level, $|P_{fi}|^2$ displays an additional node at an interior point in the zone: at about $k_\perp \sim 0.85\Gamma L$ in the case of Λ_1 and $k_\perp \sim 0.5\Gamma L$ in the case of Λ_3. This phenomenon is termed a hybridization node and will be discussed further in Sec. III E.

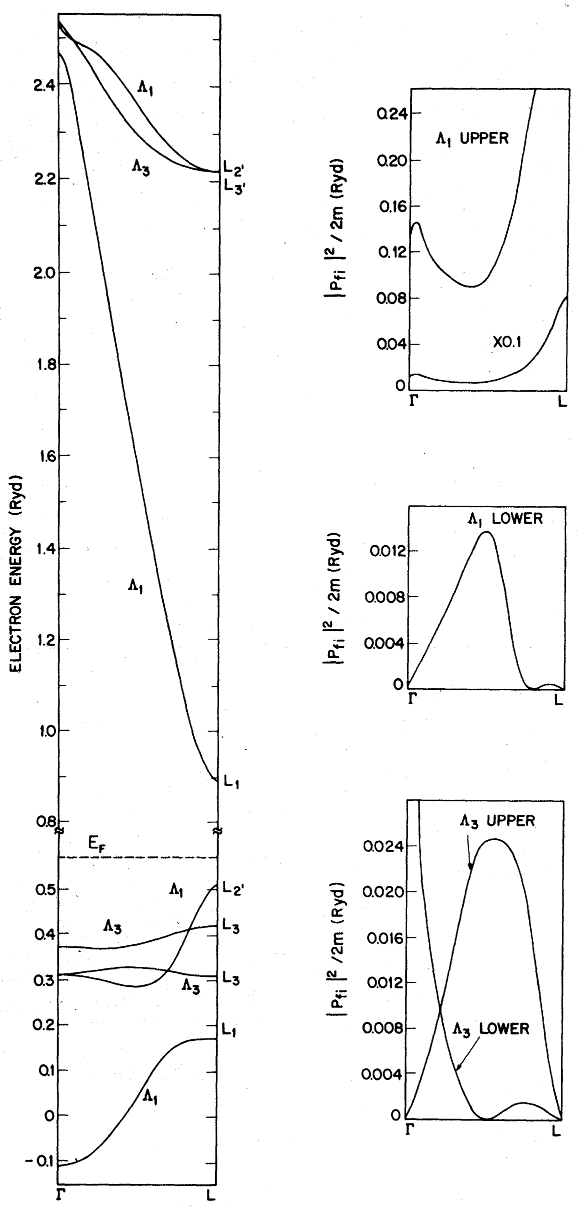

FIG. 3. Band structure of Cu and momentum matrix elements along the [111] direction. The panels on the right show the variation with $k_\perp$ of $|P_{fi}|^2$ for transitions from the initial-state bands indicated to final states in the lower unoccupied Λ_1 band. For the Λ_1 initial states we have $\vec{P}_{fi} \parallel [111]$; for the Λ_3 initial states we have $\vec{P}_{fi} \perp [111]$.

The calculated band structure along ΓX, corresponding to normal emission from the (100) surface, is shown in Fig. 4. Unlike the situation along ΓL, there are a number of unoccupied bands in the range 0.8–2.2 Ry. The bands of Δ_5 and $\Delta_{2'}$ symmetry can be eliminated since they correspond to states with zero escape probability. The actual wave functions corresponding to these states are as follows:

$$\begin{aligned}\psi(\Delta_{2'}) &= \tfrac{1}{2}(\psi_1 - \psi_2 + \psi_3 - \psi_4)\,,\\ \psi(\Delta_5) &= \tfrac{1}{2}(\psi_1 + \psi_2 - \psi_3 - \psi_4)\,,\\ \psi(\Delta_5) &= \tfrac{1}{2}(\psi_1 - \psi_2 - \psi_3 + \psi_4)\,,\end{aligned} \tag{7}$$

where ψ_1, ψ_2, ψ_3, and ψ_4 are, respectively, the plane waves with vectors $\vec{k} + \vec{G}_{\bar{1}\bar{1}\bar{1}}$, $\vec{k} + \vec{G}_{\bar{1}\bar{1}1}$, $\vec{k} + \vec{G}_{\bar{1}11}$, and $\vec{k} + \vec{G}_{\bar{1}1\bar{1}}$. None of these waves is propagating normal to the surface, and so cannot match to an external wave in the normal direction. This leaves the two bands of Δ_1 symmetry. We shall refer to these as the final-state bands. The lower of the final-state Δ_1 bands occurs at 1.152 Ry at X; close to X its wave function is composed primarily of the plane waves $\vec{k}$ and $\vec{k} + G_{\bar{2}00}$, both of which are propagating normal to the surface; escape probability is therefore high. At higher energies this band hybridizes with the other final-state Δ_1 band. In the absence of hybridization this second Δ_1 band would cross the first at about 2.3 Ry and $k_\perp \sim 0.3\Gamma X$, and would have the wave function

$$\psi(\Delta_1) = \tfrac{1}{2}(\psi_1 + \psi_2 + \psi_3 + \psi_4)\,, \tag{8}$$

which (like $\Delta_{2'}$ and Δ_5) is of zero-escape-probability form. At energies above about 2.3 Ry, the high escape character will follow the upper Δ_1 band.

Matrix elements for transitions into the upper and lower final-state Δ_1 bands are represented, respectively, by the dashed and full curves in the right-hand parts of Fig. 4. Results are for the initial state Δ_1 and Δ_5 bands; transitions from the Δ_2 and $\Delta_{2'}$ bands have zero matrix elements for all $k_\perp$, in accordance with atomic dipole selection rules to be discussed in Sec. III D. As indicated above, the high photoelectron-escape character follows the dashed curves in Fig. 4 for $k_\perp \lesssim 0.3\Gamma X$ and the full curves for $k_\perp \lesssim 0.3\Gamma X$. The interesting behavior in some of the curves which occurs at $k_1 \lesssim (0.2–0.4)\Gamma X$ is associated with the hybridization effects between the two final-state Δ_1 bands. The zero value of $|P_{fi}|^2$ for transitions from the lower initial-state Δ_1 band into the lower final-state Δ_1 band which occurs at $k_\perp \sim 0.7\Gamma X$ is attributed to a hybridization node of the kind discussed in Sec. III E.

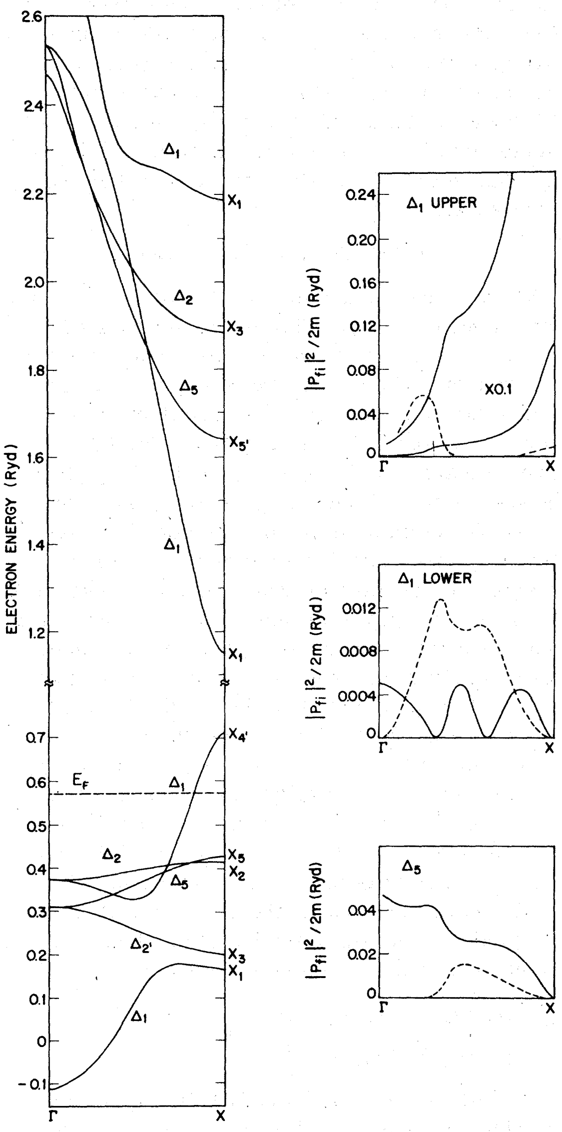

FIG. 4. Band structure of Cu and momentum matrix elements along the [100] direction. The full (dashed) curves in the panels on the right show the variations with $k_\perp$ of $|P_{fi}|^2$ for transitions from the initial-state bands indicated to final states to the third (fourth) bands of Δ_1 symmetry. For the Δ_1 initial states we have $\vec{P}_{fi} \parallel [100]$; for the Δ_5 initial states we have $\vec{P}_{fi} \perp [100]$.

D. Atomic-dipole selection rules

Some of the qualitative features of the momentum matrix element variations shown in Figs. 3 and 4 can be understood in terms of elementary atomic-dipole selection rules. From here on let us always take the z axis along the surface normal. The group representations corresponding to the [001] and [111] directions for the d orbitals are indicated in Table III. The two doubly degenerate Λ_3 states have the same sym-

TABLE III. Symmetry representations of the d orbitals appropriate to the [001] and [111] directions, and grouped according to magnetic quantum number m.

$\hat{z}\parallel[001]$	d orbital	$\hat{z}\parallel[111]$
	$m=0$	
Δ_1	$3z^2-r^2$	Λ_1
	$m=1$	
Δ_5	yz	Λ_3
	zx	upper
	$m=2$	
$\Delta_{2'}$	xy	Λ_3
Δ_2	x^2-y^2	lower

metry and are therefore allowed to mix; the distinction indicated in Table III in this case is therefore not exact; the upper Λ_3 band is predominantly of yz and zx character but has a small admixture of xy and x^2-y^2, and vice versa for the lower Λ_3 band. The unoccupied Λ_1 band and the lower final-state Λ_1 band are s-like at the zone boundary (L_1 and X_1 levels), but become progressively more p_z-like on moving into the zone. As mentioned earlier, the s-like final-state character at the zone boundary accounts for the zero matrix elements from the predominantly d-like initial states X_1, X_3, X_2, X_5, L_1, and L_3. Within the zone where the p_z character becomes stronger, we expect: a strong matrix element from the d band of $3z^2-r^2$ symmetry having $\vec{P}_{fi}\parallel\hat{z}$; a weaker matrix element from yz and zx with $\vec{P}_{fi}\parallel\hat{y}$ and $\vec{P}_{fi}\parallel\hat{x}$, respectively; zero matrix element from xy and x^2-y^2. The numerical results of Figs. 3 and 4, and in particular the zero matrix elements for $\Delta_{2'}$ and Δ_2, are consistent with these expectations.

These atomic-dipole-selection-rule considerations have been anticipated, and used with empirical success by Shevchik and co-workers.[10] They propose that the momentum matrix elements be expressed in the form

$$\vec{P}_{fi}=Au_{zx}\hat{x}+Bu_{yz}\hat{y}+Cu_{3z^2-r^2}\hat{z}+Du_s\hat{z}\,, \tag{9}$$

where u_{zx}, u_{yz}, and $u_{3z^2-r^2}$ represent components in the eigenvector of the state $|i\rangle$; u_s is the corresponding s component and, for present purposes, may be equated to the component of the lowest plane wave $|\vec{k}\rangle$. This expression goes beyond the simple plane-wave final-state approximation in which only the last two terms of Eq. (9) would be permitted. A, B, C, and D and their dependences on $\vec{k}$ are treated as disposable by Shevchik *et al.* As stated above, our results are consistent with Eq. (9). The important difference between our approach and that of Shevchik *et al.* is that this behavior arises as a natural consequence of Eq. (4) and does not require the introduction of any new disposable parameters.

The success of the present approach in its consistency with Eq. (9) appears to be in disagreement with certain conclusions of Shevchik and Liebowitz.[11] They argue that an orthogonalized-plane-wave (OPW) approach for the final states will be inadequate, just as a single-plane-wave approach is. The present scheme however is based on the OPW method. The omission in the argument of Ref. 11 is that while it considers orthogonalization to *core* levels, it takes no account of orthogonalization and hybridization with the *valence d* states. It is these effects, represented explicitly in Eqs. (2) and (3), which are crucial in the successful operation of the present scheme.

E. Hybridization nodes and minima

We have remarked upon the zeros and minima which occur in $|P_{fi}|^2/2m$ at certain points in k space. These are termed "hybridization nodes" for reasons which will now be explained. The nodes are particularly conspicuous in the transitions from the lower Δ_1 and Λ_1 bands. These are both strongly hybridized bands being plane-wave-like near Γ and progressively more and more d-like on approaching the zone boundary. We therefore expect the momentum matrix element to consist of two channels, associated with the two kinds of wave-function character. The relative amplitudes of the two channels will vary with k, and if they are of opposite sign, it is possible that there will be a point in the zone where the momentum matrix element changes sign, giving rise to a hybridization node. This explanation is essentially correct, but the details are more complicated, as will be seen below from an analysis of the actual numerical results for the Δ_1 transitions.

The wave functions in the lower initial-state Δ_1 band and the lower final-state Δ_1 band may be reasonably approximated as follows:

$$\begin{aligned}|i\rangle&=u_k|\vec{k}\rangle+u_d|d_{3z^2-r^2}\rangle,\\|f\rangle&=v_k|\vec{k}\rangle+v_{k+G}|\vec{k}+\vec{G}\rangle\,.\end{aligned} \tag{10}$$

In evaluating $\langle f|\vec{P}|i\rangle$ there will be four channels of which we shall consider only the following three:

$$\begin{aligned}p_1&=u_kP_{k,k+G}v_{k+G}\\p_2&=u_dP_{d,k+G}v_{k+G}\\p_3&=u_dP_{d,k}v_k\,.\end{aligned} \tag{11}$$

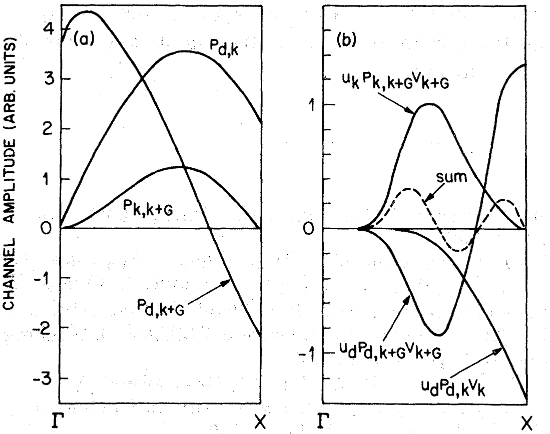

FIG. 5. Amplitudes of various components and channels in the momentum matrix element for transitions from the lowermost Δ_1 band to the high-escape-probability final-state Δ_1 band.

The P's represent the elements of the momentum operator between the basis states $|\vec{k}\rangle$, $|\vec{k}+\vec{G}\rangle$, and $|d_{3z^2-r^2}\rangle$. Their variations with $k_\perp$ are shown in Fig. 5(a). Well away from the zone boundary, v_k is small, so we can limit the discussion to p_1 and p_2. The coefficients u_k and u_d are of opposite sign (whereas $P_{k,k+G}$ and $P_{d,k+G}$ have the same sign provided $k_\perp \lesssim 0.75\Gamma X$). There is therefore a destructive interference which is directly responsible for the minimum at $k_\perp \sim 0.7\Gamma X$ in the combined matrix element shown in Fig. 5(b). The situation is complicated, however, by the fact the $P_{k,k+G}$ changes sign at slightly higher $k_\perp$.

Near the zone boundary, the initial state band is predominantly d-like so that we may neglect u_k and limit discussion to p_2 and p_3 of Eq. (11). The coefficients v_k and v_{k+G} are of the same sign, and at X they are equal. This is the well known s-like combination of the X_1 level. The values of $P_{d,k}$ and $P_{d,k+G}$ are equal and opposite at X, giving rise to a zero matrix element. The zero matrix element expected on the basis of atomic-dipole selection rules between d and s states may therefore be alternatively thought of as a hybridization node, where the hybridization occurs between the plane waves $|\vec{k}\rangle$ and $|\vec{k}+\vec{G}\rangle$ in the final state.

The combined matrix element $p_1+p_2+p_3$, shown as the dashed curve in Fig. 5(b), accounts for the basic shape of $|P_{fi}|^2/2m$ as shown in Fig. 4. It is clear, however, that other channels must also contribute since $p_1+p_2+p_3$ crosses zero twice (once at $k_\perp = 0.58\Gamma X$ and $0.77\Gamma X$), whereas there is only one minimum at $k_\perp \sim 0.7\Gamma X$ in the complete results of Fig. 4. (The additional minimum for Δ_1 in Fig. 5 at $k_\perp \sim 0.3\Gamma X$ is attributed to another hybridization node associated with the hybridization of the two final state Δ_1 bands.)

The basic requirement for a hybridization node is two hybridizing bands whose wave functions form symmetric and antisymmetric combinations. Then, depending on the relative sign of the corresponding P's, the matrix element for transitions from one of these bands is likely display a node or minimum. Since such circumstances are quite commonplace, we expect hybridization nodes to be distributed quite frequently throughout the Brillouin zone. They can be associated with either final-state or initial-state hybridizing bands. It would be of considerable interest to hunt for these nodes experimentally.

There is an effect which will tend to prevent the experimental observation of hybridization nodes. This is the lack of strict conservation of $k_\perp$ due to the fact that the surface breaks translational symmetry perpendicular to the surface. If the smearing along $k_\perp$ is not too severe, the hybridization nodes should survive and be observable as minima.

IV. CONDLUDING REMARKS

We have described in this paper a computational scheme which promises to be very useful in the interpretation of angle-resolved photoemission spectra from d-band metals. The next obvious step is to calculate some theoretical spectra and compare with experiment. This work is in progress and will be reported in due course.

Although our emphasis has been on normal emission, the scheme can be just as readily applied to off-normal emission. In this case the following considerations concerning the plane-wave decomposition of the final state will come into play. In the combined interpolation scheme, the wave functions of the unoccupied states are predominantly plane-wave-like, and may be written

$$|f\rangle = \sum_G u_{k+G} |\vec{k}+\vec{G}\rangle . \qquad (12)$$

The coefficients u_{k+G} are generated by the scheme as components of the eigenvectors. For each plane wave there is the possibility of matching onto a running wave in the vacuum and thus generating an observable photoelectron. The coefficients u_{k+G} will enter into the relative intensities of these contributions; it would be of interest to investigate how these predicted intensities compare with experiment.

ACKNOWLEDGMENTS

I am indebted to J. F. Janak for supplying the energy eigenvalues of the Cu band-structure calculation of Ref. 4. I am pleased to acknowledge also the continuing advice and encouragement of L. F. Mattheiss.

---

[1] N. V. Smith and L. F. Mattheiss, Phys. Rev. B 9, 1341 (1974).

[2] N. V. Smith, Phys. Rev. B 9, 1365 (1974); other papers in the series include M. M. Traum and N. V. Smith, Phys. Rev. B 9, 1353 (1974); J. E. Rowe and N. V. Smith, Phys. Rev. B 10, 3207 (1974).

[3] See, for example, *Photoemission and the Electronic Structure of Surfaces*, edited by B. Feuerbacher, B. Fitton, and R. F. Willis (Wiley, New York, 1978); *Photoemission in Solids I General Principles*, Topics in Applied Physics Series, edited by M. Cardona and L. Ley (Springer-Verlag, Berlin, 1978), Vol. 26.

[4] J. F. Janak, A. R. Williams, and V. L. Moruzzi, Phys. Rev. B 11, 1522 (1975).

[5] L. Hodges, H. Ehrenreich, and N. D. Lang, Phys. Rev. 152, 505 (1966); F. M. Mueller, Phys. Rev. 153, 659 (1967).

[6] E. I. Blount, in *Solid State Physics*, edited by F. Seitz and D. Turnbull (Academic, New York, 1962), Vol. 13, p. 305.

[7] G. Dresselhaus and M. S. Dresselhaus, Phys. Rev. 160, 649 (1967); D. D. Buss and V. E. Schirf, in *Electronic Density of States*, Natl. Bur. Stand. Special Publication No. 323, edited by L. H. Bennett (U.S.G.P.O. Washington, D. C., 1971), p. 115.

[8] P. O. Nilsson, in *Solid State Physics*, edited by H. Ehrenreich, F. Seitz, and D. Turnbull (Academic, New York, 1974), Vol. 29, p. 139.

[9] D. Beaglehole and E. Erlbach, Solid State Commun. 8, 255 (1970).

[10] N. J. Shevchik and D. Liebowitz, Phys. Rev. B 18, 1618 (1978); D. Liebowitz and N. J. Shevchik, Phys. Rev. B 18, 1630 (1978); M. Sagurton and N. J. Shevchik, Phys. Rev. B 17, 3859 (1977).

[11] N. J. Shevchik and D. Liebowitz, Phys. Rev. B 16, 2395 (1977).